



Publication Year	2016
Acceptance in OA	2020-05-12T08:38:42Z
Title	Chromophores from photolyzed ammonia reacting with acetylene: Application to Jupiter's Great Red Spot
Authors	Carlson, R. W., Baines, K. H., Anderson, M. S., FILACCHIONE, GIANRICO, Simon, A. A.
Publisher's version (DOI)	10.1016/j.icarus.2016.03.008
Handle	http://hdl.handle.net/20.500.12386/24721
Journal	ICARUS
Volume	274

1 **Chromophores from photolyzed ammonia reacting with acetylene:**
2 **Application to Jupiter's Great Red Spot**

3
4 R. W. Carlson*,¹ K. H. Baines¹, M. S. Anderson¹, G. Filacchione², A. A. Simon³

5
6 ¹ Jet Propulsion Laboratory, California Institute of Technology, Pasadena, California, USA

7 ² Istituto di Astrofisica e Planetologia Spaziali, Roma, Italy

8 ³ NASA Goddard Space Flight Center, Greenbelt, Maryland USA

9
10 * Corresponding Author

11
12 Mailing address:

13
14 Robert W. Carlson

15 Mail Stop 183-601

16 Jet Propulsion Laboratory

17 4800 Oak Grove Dr.

18 Pasadena, CA 91109

19 Phone: 818-354-2648

20 E-Mail: Robert.W.Carlson@jpl.nasa.gov

21
22 Manuscript pages: 20

23 Figures: 6

24 Tables: 1

25
26 Keywords: Jupiter, atmosphere; Photochemistry, Atmospheres, chemistry,

27 Atmospheres, composition, Organic chemistry

28

29 **Abstract**

30

31 The high altitude of Jupiter's Great Red Spot (GRS) may enhance the upward flux of
32 gaseous ammonia (NH_3) gas into the high troposphere, where NH_3 molecules can be
33 photodissociated and initiate a chain of chemical reactions with downwelling acetylene
34 molecules (C_2H_2). These reactions, experimentally studied earlier by Ferris and Ishikawa
35 (1987; 1988), produce chromophores that absorb in the visible and ultraviolet regions.
36 In this work we photolyzed mixtures of NH_3 and C_2H_2 using ultraviolet radiation with a
37 wavelength of 214 nm and measured the spectral transmission of the deposited films in
38 the visible region (400-740nm). From these transmission data we estimated the
39 imaginary indices of refraction. Assuming that ammonia grains at the top of the GRS
40 clouds are coated with this material, we performed layered sphere and radiative
41 transfer calculations to predict GRS reflection spectra. Comparison of those results with
42 observed and previously unreported *Cassini* visible spectra and with true-color images
43 of the GRS show that the unknown GRS chromophore is spectrally consistent with the
44 coupled NH_3 - C_2H_2 photochemical products produced in our laboratory experiments.
45 Using high-resolution mass spectroscopy and infrared spectroscopy we infer that the
46 chromophore-containing residue is composed of aliphatic azine, azo, and diazo
47 compounds.

48

49 **1. Introduction**

50

51 Jupiter is colored using a basic palette of white, yellows, and browns (Peek, 1958; Taylor
52 et al., 2004) for the belts, zones, and also for many of the vortex features. However for
53 Jupiter's largest storm, the Great Red Spot (GRS), a deep orange, almost red, pigment is
54 additionally found. The identities of the chromophores that produce Jupiter's colors are
55 still unknown although many suggestions have been advanced (see reviews by Sill
56 (1975) and West et al.(1986)). The three main candidates at present, all potentially
57 produced by ultraviolet photolysis in the jovian atmosphere, are (1) organic molecules
58 (Sagan and Miller, 1960; Sagan et al., 1967; Woeller and Ponnampereuma, 1969; Sagan
59 and Khare, 1971; Khare and Sagan, 1973; Ferris and Chen, 1975; Ponnampereuma, 1976;
60 Ferris and Morimoto, 1981; Ferris and Ishikawa, 1987; Ferris and Ishikawa, 1988), (2) red
61 phosphorous from phosphine photolysis (Prinn and Lewis, 1975; Ferris and Benson,
62 1981; Ferris et al., 1982; Ferris et al., 1984; Ferris and Khwaja, 1985; Guillemin et al.,
63 1995; Guillemin et al., 1997; Guillemin et al., 2001), and possibly (3) hydrogen and
64 ammonium polysulfides and elemental sulfur (Owen and Mason, 1969; Lewis and Prinn,
65 1970; Prinn, 1970) although these were suggested for lower troposphere
66 chromophores.

67

68 A possible clue to the production of the GRS chromophore is the great height of this
69 storm, being one of the tallest vortex features on the planet. This was illustrated using
70 Galileo Near Infrared Mapping Spectrometer (NIMS) spectral mapping (Baines et al.,
71 1996; Irwin et al., 1999) and Solid State Imaging (SSI) data (Simon-Miller et al., 2001a).
72 Analysis of NIMS observations, illustrated in Fig. 1 and described in the Appendix, show
73 that the GRS cloudtop extends about 6 km above the main ammonia (NH₃) cloud deck,
74 reaching pressure levels of approximately 200 mbar.

75

76 It is often postulated that the GRS vortex upwells gas from below. At the 700-mbar
77 level, the GRS shows an enhancement in the NH₃ mixing ratio (Sada et al., 1996). At
78 higher altitudes, at the 550-mbar to 380-mbar levels, little enhancement is found
79 relative to adjacent regions (Lara et al., 1998; Fletcher et al., 2010) although Achterberg
80 et al. (2006) suggest a measurable increase at 438 mbar. Above the 300 mbar level a
81 relative depletion is found for the GRS (Tokunaga et al., 1980; Griffith et al., 1992;
82 Edgington et al., 1999) as well as a much steeper gradient (Tokunaga et al., 1980; Irwin
83 et al., 2004), consistent with upward flow of gaseous NH₃ and loss by photodissociation
84 and condensation.

85

86 At the high altitudes of the GRS, solar ultraviolet radiation with wavelengths $> \sim 200$ nm
87 can penetrate and dissociate NH_3 molecules as $\text{NH}_3 + h\nu \rightarrow \text{NH}_2 + \text{H}$ (Prinn, 1970;
88 Visconti, 1981; Cheng et al., 2006). The altitude (pressure) for maximum absorption rate
89 is approximately 200-250 mbar for a solar zenith angle of zero and increases for non-
90 normal illumination. In this altitude range acetylene, produced higher up by shorter
91 wavelength solar ultraviolet-initiated photochemistry, diffuses down and is destroyed
92 by reactions with amino radicals (NH_2) and atomic hydrogen and by other
93 photochemical processes (Kaye and Strobel, 1983; Moses et al., 2010).

94

95 Mixtures of gaseous acetylene and ammonia are known to react under NH_3 photolysis
96 and produce - in addition to HCN - a condensate that absorbs radiation in the ultraviolet
97 and visible region (Ferris and Ishikawa, 1987; Ferris and Ishikawa, 1988), however
98 measurements of the spectral absorption properties of this potential chromophore are
99 not available (see summary of prior related work in Section 2, below). Furthermore,
100 there are few spectra of the GRS in the literature. In this work we extend the ammonia -
101 acetylene photolysis experiments (Section 3) and obtain the imaginary index of
102 refraction of the colored condensate. Employing electromagnetic scattering theory for
103 layered spheres and radiative transfer calculations we simulate reflection spectra of the
104 GRS (Section 4). We then compare our laboratory results to newly analyzed *Cassini*
105 visible spectra, *Hubble Space Telescope* (HST) data, and ground-based measurements.
106 We discuss the composition of the chromophore-containing residue using mass and
107 infrared spectroscopic measurements work and suggest potential observational tests
108 (section 5). Jovian photochemical flux considerations and possible relations to other red
109 features in Jupiter's atmosphere are briefly discussed in Section 6.

110

111 **2. Prior Studies of Ammonia-Acetylene Gases and related Reactions**

112

113 Ammonia + Methane

114 The early jovian chemical simulations used electrical discharges and are of interest here
115 because acetylene is produced and the ultimate reaction products may be similar to the
116 present experiments. Sagan and Miller (1960) electrically sparked a methane, ammonia,
117 and hydrogen gas mixture and produced ethane (C_2H_6), ethylene (C_2H_4), acetylene
118 (C_2H_2), hydrogen cyanide (HCN), and acetonitrile (CH_3CN).

119

120 In a series of experiments by Ponnampereuma and colleagues, the products produced by
121 electrical discharges in ammonia and methane gases were studied, first finding
122 production of HCN, nitriles, and reddish-brown solid residues (Woeller and
123 Ponnampereuma, 1969). Acid hydrolysis of the residues gave amino and imino acids
124 (Chadra et al., 1971) and Molton and Ponnampereuma (1974) performed mass
125 spectroscopic studies of the condensed products, with their results suggesting the
126 formation of aminonitriles.

127

128 Ferris and coworkers (Ferris and Chen, 1975; Ferris and Morimoto, 1981; Ferris et al.,
129 1982) studied the photolysis of NH_3 in the presence of CH_4 wherein the hot hydrogen
130 atoms liberated by 185-nm photons possessed sufficient kinetic energy to overcome the
131 0.6 eV reaction barrier of CH_4 , producing the methyl radical. Subsequent reactions
132 yielded C_2 - and C_3 -hydrocarbons, methylamine (CH_3NH_2) and hydrogen cyanide (HCN), as
133 well as H_2 , N_2 and hydrazine (N_2H_4). This mechanism for chemical destruction of CH_4 is
134 unlikely to be prevalent on Jupiter due to thermalization of the energetic H atoms by the
135 dominant H_2 gas (Ferris and Morimoto, 1981; Ferris et al., 1982).

136

137

Ammonia + Acetylene

138 Kaye and Strobel (1983) first suggested that HCN is formed in Jupiter's atmosphere from
139 photolyzed NH_3 reacting with acetylene and Moses et al. (2010) recently performed a
140 comprehensive model of Jupiter's coupled NH_3 - C_2H_2 photochemistry. The initial
141 production of molecules containing carbon and nitrogen can occur in several path ways,
142 beginning when ammonia is photodissociated into NH_2 + H. The amino radical (NH_2) can
143 react with C_2H_2 in a three-body reaction. Additionally, the liberated hydrogen atoms
144 react with C_2H_2 and its reaction products, forming C_2H_3 and other radicals, which react
145 with NH_2 to form N-containing hydrocarbons.

146

147 An early study by Tsukada et al. (1972) indicated that the heterocyclic molecule pyrrole
148 ($\text{C}_4\text{H}_4\text{NH}$) was formed in NH_3 - C_2H_2 photolysis. Comprehensive investigations of the
149 photochemistry of NH_3 + C_2H_2 were performed by Ferris and Ishikawa (1987; 1988), who
150 demonstrated HCN production and suggested that this molecule is formed from the
151 intermediate products acetaldazine ($\text{CH}_3\text{CH}=\text{N}-\text{N}=\text{CHCH}_3$) and subsequent acetonitrile
152 (CH_3CN). An ultraviolet absorbing brownish residue formed with infrared spectral
153 characteristics dissimilar to acetylene polymers, but instead showed CH stretch bands of
154 the methyl and methylene functional groups, indicating the presence of saturated

155 aliphatic hydrocarbons. The presence of –NH and –NH₂ groups was indicated by the NH
156 stretch feature at 3300 cm⁻¹.

157

158 The coupled photochemistry of NH₃ and C₂H₂ was further studied and numerous
159 intermediate and final reaction products (e. g., azines, imines, amines, nitriles, and
160 others) and their quantum yields determined Keane (1995) . This work enabled
161 predictions to be made for the Galileo entry probe mass spectrometer measurements
162 (Keane et al., 1996) and formed the experimental basis for a comprehensive model of
163 jovian ammonia-acetylene photochemistry (Moses et al., 2010).

164

165 **3. Photolysis Measurements**

166

167 Our experiments were similar to those performed by Ferris and Ishikawa (1987; 1988),
168 using ammonia and acetylene in different proportions but we also added methane in
169 some experiments. The experiments were performed at ambient temperatures. A
170 cartoon illustrating the experimental apparatus and their arrangement is shown in Fig.
171 2.

172

173 The NH₃ and C₂H₂ gases were both from Matheson with purities of 99.999% and 99.6%,
174 respectively. The C₂H₂ sample, as delivered, was dissolved in acetone (CH₃COCH₃) but
175 was further purified by repeated vacuum distillation, with the acetone content
176 measured by mass spectroscopy using a quadrupole residual gas analyzer (RGA). Typical
177 acetone levels achieved were < 0.1% mole fraction relative to C₂H₂. The methane gas
178 was from Airgas and of ultrahigh purity grade (99.99%). The gases were mixed in a 300-
179 ml stainless steel high-vacuum manifold and connected to the photolysis cell with a
180 Viton O-ring seal with a low-vapor pressure (5×10^{-13} Torr) tetrafluorethylene grease.
181 The system was operated as a closed system except for occasional gas sampling for
182 infrared and mass spectra monitoring. The large manifold volume relative to the volume
183 of the photolysis cell enabled us to generate measurable amounts of photolysis
184 products, limited only by its ultraviolet absorption.

185

186 We used a Zn lamp (UV Products) that emits ultraviolet (UV) radiation in three lines at
187 wavelengths $\lambda = 202.5, 206.2,$ and 213.9 nm with measured relative intensities of 1, 2,
188 and 100 respectively. The UV energy flux incident on the cell window was about 10 mW
189 or 10^{16} 214-nm photons s⁻¹. Photolysis at this flux rate occurs at the beginning of the
190 irradiation but the rate decreased rapidly as the ultraviolet- and visible-absorbing film

191 formed. Although C_2H_2 can be photodissociated in this near-threshold region (Mordaunt
192 et al., 1998), the absorption cross sections (Nakayama and Watanabe, 1964) are small
193 compared with those of ammonia (Chen et al., 1999) and we estimate that less than
194 1/500 of the UV photons are absorbed by C_2H_2 in the mixtures used here. The photolysis
195 cells were 25- and 50-mm long, 19-mm inside diameter glass cells with UV-grade quartz
196 windows. No spectral differences were found for films made with different length cells.
197 Similar films were also made using a Teflon cell with CaF_2 windows.

198

199 We periodically measured the spectral transmission of the films as they developed with
200 time. Prior to the start of the irradiations the photolysis cell was placed in the optical
201 path between a tungsten-halogen incandescent source and a grating spectrometer.
202 Radiation from this lamp was collimated with a CaF_2 lens, passed through the cell and an
203 optical filter transmitting radiation for $\lambda > 400$ nm, and then focused with a second CaF_2
204 lens to image the lamp's filament on the spectrometer's entrance slit. The spectrometer
205 was an Acton 0.5-m Czerny-Turner mount with a 1200 lines/mm grating. Reference
206 spectra in the 400 to 740-nm interval with a resolution of 4 nm were obtained of the
207 evacuated cell. The cell was then filled with a mixture of C_2H_2 and NH_3 gas, and, in some
208 cases, CH_4 . Guided by the work of Ferris and Ishikawa (1987; 1988), the initial NH_3 to
209 C_2H_2 molar ratio was generally $\sim 10:1$ with an $NH_3 + C_2H_2$ pressure of ~ 120 Torr (158
210 mbar), although some experiments were performed at a lower molar ratio and total
211 pressures (Table 1). A 10:1 molar ratio of NH_3 to C_2H_2 occurs at approximately the 130
212 mbar level in the jovian atmospheric model of Moses et al. (2010) and is within the 100
213 – 160 mbar region where most of the initial production of the carbon- nitrogen
214 molecules occurs (see the supplementary information of Moses et al., 2010). The partial
215 pressures are orders of magnitude higher in the laboratory measurements compared to
216 NH_3 and C_2H_2 in Jupiter's upper troposphere, but the total pressure is comparable so 3-
217 body reactions would be expected to occur at approximately the same rates. When CH_4
218 was added its partial pressure was about twice greater than that of NH_3 . Spectra of the
219 filled but un-irradiated cell were then obtained, and showed no change from the empty-
220 cell spectra, as expected. The UV lamp was then positioned and irradiation begun. At
221 intervals that increased with time the photolysis lamp removed and transmission
222 spectra were obtained.

223

224

225

226

227

228 Table 1. Summary of major experiments

No.	System	Molar ratios	Total pressure, Torr	Notes
1	NH ₃ + C ₂ H ₂	10:1	124	UV-Vis absorption
2	NH ₃ + C ₂ H ₂	5:1	130	“ “ “
3	NH ₃ + C ₂ H ₂	10:1	93	“ “ “
4	NH ₃ + CH ₄	1:2	118	No apparent reaction
5	NH ₃ + C ₂ H ₂ + CH ₄	10:1:20	122	Similar to NH ₃ + C ₂ H ₂ cases
6	NH ₃ + C ₂ H ₂	12:1	15	With SiO ₂ powder

229

230 During irradiation an absorbing film developed on the inner surface of the irradiated
231 window. The growth rate of the film and its transmission diminished with time as the
232 film's thickness and corresponding UV opacity increased. At the same time, mass
233 spectrometer measurements showed that the acetylene fraction, relative to ammonia,
234 decreased although the total manifold pressure remained about the same, presumably
235 from the generation of N₂, H₂, HCN, and other products, consistent with mass spectra
236 and infrared spectra of a condensed sample of the manifold gas (Section 5).

237

238 The films showed evidence for interference fringes (channel fringes) with amplitude
239 modulations of approximately $\pm 4\%$ and a period of $\sim 5000 \text{ cm}^{-1}$ indicating films of ~ 1
240 μm in optical thicknesses or $\sim 0.7 \mu\text{m}$ in physical thickness using a refractive index of $n =$
241 1.4 (a typical value for aliphatic hydrocarbons). In order to minimize this modulation
242 effect on the spectra we performed an average of three successive spectra, using the
243 changing phase to form an average with muted oscillations (see Fig. 3A). Even with this
244 averaging, it is difficult to accurately estimate the wavelength-independent extinction
245 coefficient, which could also contain a scattering component. In general the spectra
246 show less modulation but some still show the effect (e. g., for the 15-, 108-, and 197-
247 hour average irradiation times). Nevertheless, the trend and spectral shape are
248 indicated and typical of all of our NH₃ + C₂H₂ experiments.

249

250 Transmission spectra taken at the end of the irradiation were followed by evacuation of
251 gas from of the cell and another transmission spectrum was obtained. No change was
252 observed from the preceding spectrum, showing that the film material was non-volatile.
253 A spectrum taken after air exposure similarly showed no change, indicating chemical

254 stability. A comparison of the lamp spectra without the cell in the path showed no
255 change in the spectral shape to within 3%.

256

257 Addition of methane to $\text{NH}_3 + \text{C}_2\text{H}_2$ (Experiment No. 5) still produced a film with the
258 same color and transmission properties. The growth rate was little affected by added
259 CH_4 . An experiment with no acetylene but only NH_3 and CH_4 did not produce any
260 measurable absorption, as expected owing to the CH_4 reaction barrier.

261

262 The films that are produced are yellow in reflection and pale orange in transmission.
263 They are limited in thickness by their absorbance in the photolyzing ultraviolet region.
264 As the films grew, the amount of transmitted ultraviolet radiation and the resulting
265 growth rate diminished rapidly. In order to produce more opaque films, we placed a
266 millimeter-thick layer of silica powder, consisting of 10- μm diameter spheres
267 (AngstromSphere), into an absorption cell and introduced a sample of $\text{NH}_3 + \text{C}_2\text{H}_2$ gas
268 (Experiment No. 6 in Table 1). Lower partial pressures were used to ensure penetration
269 of photons well into the gas + powder medium to coat the spheres with the
270 chromophore. The cell was irradiated from below for 6 days with the cell occasionally
271 shaken to redistribute the powder and to provide fresh grain surfaces near the bottom
272 window for collection of the generated photoproducts. After irradiation, a photograph
273 (Fig. 4A) of the transmitted light was obtained using a white light emitting diode (LED)
274 lamp with a color temperature somewhat greater than that of the sun. A colored
275 pigment was found and is compared to GRS colors on the following Section.

276

277 **4. Great Red Spot Spectral and Color Comparison**

278

279 There are surprisingly few spectra of the GRS to compare with laboratory
280 measurements. Here we use observations by *Cassini's* VIMS-V (visible) channel, an
281 imaging spectrometer that covers the 300 – 1050 nm region at a spectral resolution of
282 1.46 nm and an angular resolution of $167 \mu\text{rad} \times 167 \mu\text{rad}$ per pixel (Miller et al., 1996;
283 Brown et al., 2004; Coradini et al., 2004). These spatially resolved spectra (Fig. 3B) of
284 the GRS were obtained during *Cassini's* December, 2000 flyby of Jupiter, acquired at
285 2000-339 08:31:01.684 with an integration time of 1.28 sec and denoted Cube C23
286 V1354610545. The raw data cubes are available on NASA's Planetary Data System along
287 with calibration routines. The ground calibration is described by Capaccioni et al. (1998)
288 and Filacchione (2006). The GRS was observed at a phase angle of 9.7° and within 10-
289 15° of local noon, similar to observations obtained from Earth. The spacecraft range to

290 Jupiter for this observation was 26.4×10^6 km, projecting a pixel footprint of $\sim 4,400$ km
291 $\times 4,400$ km on Jupiter, smaller than the nominal $10,000$ km $\times 25,000$ km GRS. We show
292 two spectra from this observation, the first being for the central pixel and the second
293 being the average of the central and adjacent eastern and western pixels. There is a
294 second GRS observation by *Cassini* (V1356904960), obtained with better spatial
295 resolution but at a high phase angle and not geometrically comparable to ground-based
296 and HST observations. Data from the IR portion of *Cassini* VIMS were also obtained
297 during both observations and discussed briefly in Section 5.

298

299 Fig. 3B also contains the measurements performed by Orton (1975) using a scanner at
300 fixed wavelengths, HST imagery data in several filters (Simon-Miller et al., 2001b; Pérez-
301 Hoyos et al., 2009; Strycker et al., 2011; Simon et al., 2015), and albedo values for the
302 HST image shown in Fig. 4B and discussed below.

303

304 To compare our laboratory results with observations we calculated the reflectance,
305 assuming the cloud-top ammonia particles are coated with a thin layer of chromophore,
306 although other colored aerosol formation and mixing scenarios are possible but not
307 investigated here. The grains are assumed spherical with a log-normal distribution of
308 radii and an average diameter of $1 \mu\text{m}$. Optical constants for the chromophore were
309 found using the 70-hour transmission data (Fig. 3A) with the thickness and assumed
310 value of real index noted earlier. Data from Martonchik et al. (1984) for were used for
311 the NH_3 optical constants. Mie calculations for layered spheres (Toon and Ackerman,
312 1981) were performed for layer thicknesses of $\delta R/R = 1/100, 2/100, 4/100, 6/100,$ and
313 $16/100$. Using the calculated single scattering albedos and asymmetry parameters, we
314 employing similarity relations (Van De Hulst, 1980; Hapke, 1993) to find the equivalent
315 single scattering albedo for isotropic scattering and the reflectance for a semi-infinite
316 cloud using the formulation of Hapke (1993). Rayleigh scattering and extinction were
317 included. In order to compare these results with observations performed at different
318 times and different GRS colors, we normalized the observations and computed spectra
319 to a value of 0.83 at 673 nm, approximating typical I/F values for Jupiter at that
320 wavelength (I is the observed radiance and πF is the solar irradiance). The results are
321 shown in Fig. 3B. The computed spectra, although approximate, mimic the general trend
322 indicated by the ground and HST-derived data and the *Cassini* spectra.

323

324 A color comparison is shown on Fig. 4, where we have used a HST images obtained in
325 June 2008 (Program GO11498) and compare a true color image to a photograph of the

326 coated silica particles of Experiment No. 6. The HST color image in Fig. 4B uses absolute
327 I/F values at red (673 nm), green (502 nm), and blue (410 nm) wavelengths without
328 contrast enhancement to render an image that most closely resembles the color of the
329 GRS at that time. Images were obtained at 255, 343, 375, 390, 410, 437, 469, 503, 673,
330 and 889 nm with exposure times of 230, 140, 100, 35, 8, 14, 10, 8, 4, and 40 seconds,
331 respectively. Comparison of these two images shows similar colors, and a spectral
332 comparison of the filter data obtained in the HST observation with modelled spectra
333 (Fig. 3B) indicates spectral similarities.

334

335 **5. Chromophore composition and possible HCN**

336

337 The laboratory transmission spectra do not exhibit spectral characteristics that provide
338 any chemical identification, so here we investigate the chemical composition of the
339 experimental chromophore-containing residue using two techniques, mass
340 spectroscopy and infrared spectroscopy. Mass spectroscopy can tell us which atoms are
341 present and their number, while infrared spectroscopy indicates the functional groups
342 that are present. Unique identification of the molecules present in the residue is not
343 possible with just this information but the classes of molecules can be suggested.

344

345 The mass spectroscopic measurements used open-air ionization produced by Penning
346 ionization using metastable helium ($\text{He } 2^3\text{S}$). This is coupled to a time-of-flight (TOF)
347 mass spectrometer, forming a system termed DART (Direct Analysis in Real Time, Cody et
348 al., 2005). This soft ionization enables molecules that are otherwise difficult to ionize
349 and volatilize to be readily introduced into the mass spectrometer system. The ions that
350 are produced in ambient conditions are protonated parent molecules MH^+ , where M is
351 the parent molecule and the proton arises from atmospheric water vapor. The TOF
352 spectrometer has a very wide mass range and individual masses can be measured with
353 accuracy better than 5 mDa. This enables molecular identification of specific mass peaks
354 using the variations in atomic mass among the elements and their isotopes (see below).
355 The residue was extracted with dichloromethane (CH_2Cl_2), the solvent was allowed to
356 evaporate, and the residue then exposed to the beam of excited He of the DART system,
357 forming the mass spectrum shown in Fig 5. A mass calibration run using polyethylene
358 glycol standards (PEG 600) was also performed. No oxygen-containing compounds were
359 found, indicating no contamination from acetone or atmospheric oxygen.

360

361 A diffuse reflectance infrared spectrum of the residue in KBr was also obtained (Fig. 6)
362 along with a blank sample. No spectral features of dichloromethane were found nor
363 were any features attributable to acetone or oxygen related products. The results of the
364 DART and DRIFT analyses are discussed together below.

365

366 Referring to the DART spectrum (Fig. 5), the major mass peaks form repeating groups of
367 three members with each member differing by 2 hydrogen atoms. The different number
368 of H atoms indicates different numbers of singly and multiply bonded C atoms and
369 differences in the molecules' functional groups. The group repeat interval corresponds
370 to two methylene groups, $-\text{CH}_2-\text{CH}_2-$, probably derived from C_2H_2 and the C_2H_3 , C_2H_4 ,
371 and C_2H_5 radicals from $\text{C}_2\text{H}_2 + \text{H}$ reactions (Moses et al., 2010). The number of repeats is
372 > 6 , four of which are shown in this spectrum and at least two more at higher mass but
373 of lesser intensity.

374

375 The high resolving power of the DART system enables us to resolve isotopic mass
376 differences and assign the numbers of C, H, and N atoms in the molecules for each
377 molecular mass position. ^{14}N and $^{12}\text{CH}_2$ have a mass difference of 13 mDa so one can
378 distinguish nitrogen-containing compounds from hydrocarbons and determine how
379 many N atoms are in the molecule. We determined the positions of the stronger peaks
380 between 113 Da and 170 Da and compared the observed positions with those predicted
381 for hydrocarbons containing 0, 1, 2, 3, or 4 nitrogen atoms,. The corresponding mean
382 differences between the observed and predicted positions for these cases were found
383 to be -26.1, -13.5, -1.0, 11.6, and 24.2 Da, respectively, each with a standard deviation
384 of 0.65 Da. Only positions for the two nitrogen atom case agree with the observed
385 positions. Therefore these data uniquely identify the relative number C, H, and N atoms
386 in each of the three members of a group, indicated with the molecular formulas:
387 $\text{C}_{2n}\text{H}_{4n-2}\text{N}_2$, $\text{C}_{2n}\text{H}_{4n}\text{N}_2$, and $\text{C}_{2n}\text{H}_{4n+2}\text{N}_2$. The presence of two N atoms in these
388 molecules may be related to the azine compounds ($\text{RR}'=\text{N}-\text{N}=\text{R}''\text{R}'''$, where R represents
389 hydrocarbon radicals) found by Ferris and Ishikawa (1987; 1988) and Keane (1995).

390

391 The smaller peaks that are offset by +1 Da correspond to carbon and nitrogen isotopes.
392 One can also investigate the presence of potential impurity atoms by their masses. In
393 particular the presence of oxygen atoms was investigated and no indication of its
394 presence was found.

395

396 In order to characterize these molecules and their functional groups we employ the
397 infrared spectra of the photolysis product shown in Fig. 6. We first note a broad band
398 centered at 3200 cm^{-1} where the N–H stretch band is found. For amines ($-\text{NH}_2$), there
399 are generally two peaks (the symmetric and asymmetric stretch transition, (Socrates,
400 2001)) so the appearance of a single band indicates the presence of mainly imine groups
401 ($=\text{N}-\text{H}$). At lower frequencies ($\sim 2960\text{-}2840\text{ cm}^{-1}$), the methyl ($-\text{CH}_3$) and methylene
402 ($-\text{CH}_2-$) groups indicate the presence of aliphatic hydrocarbons, mainly saturated
403 alkanes. The peak at 2056 cm^{-1} may be due to a diazo compound ($>\text{C}=\text{N}=\text{N}$, Socrates,
404 2001)) and related to the di-nitrogen compounds found by Ferris and Ishikawa and
405 Keane. The C=N stretching band of azines ($>\text{C}=\text{N}-\text{N}=\text{C}<$) is indicated in the $1650\text{-}1690$
406 cm^{-1} region and the C-N band of possible azo compounds ($\text{R}-\text{N}=\text{N}-\text{R}'$) appears at 1020
407 cm^{-1} .

408

409 The central member of the three members in each DART group is generally the most
410 abundant and we suggest its molecular formula $\text{C}_{2n}\text{H}_{4n}\text{N}_2$ to indicate alkanes with
411 azine and/or diazo groups, possibly also including alkene-azo compounds. The
412 $\text{C}_{2n}\text{H}_{4n+2}\text{N}_2$ members are possibly alkanes with an azo group. The $\text{C}_{2n}\text{H}_{4n-2}\text{N}_2$
413 members may be unsaturated alkene-azine and alkene-diazo hydrocarbons. The
414 complex that produces the chromophore activity is unknown, but some azo compounds
415 are known to produce dyes.

416

417 We briefly investigated the production of HCN by freezing out at 70 K a sample of the
418 irradiated gas and obtaining an infrared spectrum of the sample. A spectral feature was
419 found at 2118 cm^{-1} that is close to the condensed HCN position ($\sim 2100\text{ cm}^{-1}$) but its
420 definitive identification must be obtained using a gas phase spectrum. If this feature is
421 shown to be from HCN, then its possible presence over the GRS and elsewhere may
422 indicate enhanced coupling of ammonia and acetylene chemistry at high altitudes.

423

424 The 2056 cm^{-1} feature, suggested here to be from a diazo compound, would be present
425 in the GRS infrared spectra if $\text{NH}_3\text{-C}_2\text{H}_2$ photolysis produces this chromophore. We
426 examined NIMS and *Cassini* infrared spectra for such a feature. However, there are
427 strong and ubiquitous atmospheric gas absorption bands present that preclude any
428 chromophore identification at NIMS and VIMS spectral resolution.

429

430 **6. Summary and Discussion**

431

432 The production of a chromophore that provides the orange-red color to the Great Red
433 Spot may be initiated by photolysis of ammonia in the high tropospheric altitudes. The
434 photoproducts NH_2 and H then react with downwelling acetylene and initiate a chemical
435 chain, producing a solid residue that can provide color. If this is indeed the source of the
436 GRS color, the pigments may consist of aliphatic azo, diazo, or azine compounds.

437

438 Moses et al.'s (2010) study of C_2H_2 and NH_3 photochemistry in Jupiter's atmosphere
439 indicates that the coupling is weak due to the low eddy diffusion at the tropopause,
440 resulting in low C_2H_2 flux into the troposphere and consequently low chromophore
441 production. However, only a single eddy diffusion coefficient profile was used in their
442 work, but there could be spatial variations with latitude and the underlying
443 meteorological conditions. Edgington et al. (1999) found that the eddy mixing rate at
444 250 mb is greater in the GRS region compared to regions to the north and south. Similar
445 latitudinal variations were found in the same altitude region by Lara et al. (1998). It is
446 plausible that GRS vortex activity could influence the dynamical properties of the
447 atmosphere above, perhaps by the generation of upwardly propagating gravity waves.
448 The strength of such effects could vary with time and cause the observed temporal
449 variations in the GRS color.

450

451 Our experiments used gaseous NH_3 and C_2H_2 , and we have not considered the potential
452 photochemical role of ice and aerosols. NH_2 and H can be photoemitted from ammonia
453 ice grains and chemical reactions can take place on downwelled polyacetylene aerosols.
454 Such effects may be important and need quantification.

455

456 We note that other regions of Jupiter can be red, and in some cases, redder than the
457 GRS as shown by Simon-Miller et al. (2013) for the North Equatorial Belt and an unusual
458 red vortex. These features occur at lower elevations than the GRS and their spectra are
459 different from GRS spectra, suggesting that a different chromophore may be present.
460 However, it is also possible that the same chromophores are present but local
461 conditions modify their optical properties.

462

463 **Acknowledgements**

464 RWC and KHB gratefully acknowledge funding from NASA's Planetary Atmospheres
465 Program. Portions of this work were performed at the Jet Propulsion Laboratory,
466 California Institute of Technology, under contract with the National Space and
467 Aeronautics Administration. Some results were based on observations made with the

468 NASA/ESA *Cassini* spacecraft and the *Hubble Space Telescope*. Data from the latter were
469 obtained from the Data Archive at the Space Telescope Science Institute, operated by
470 the Association of Universities for Research in Astronomy, Inc., under NASA Contract
471 NAS 5-26555. These observations are associated with program GO11498.

472

473 **APPENDIX**

474 Figure 1 shows the cloudtop altitude structure of the Great Red Spot (GRS) as derived
475 from a spectral mapping mosaic acquired by the Near-Infrared Mapping Spectrometer
476 (NIMS) onboard the Galileo Orbiter on June 26, 1996 during the Galileo spacecraft's first
477 orbit. As described by Baines et al. (2002), the mosaic of the Great Red Spot and its
478 environs were acquired in 23 discrete colors from 0.74 to 5.21 μm with an average
479 spatial resolution of 730 km/pixel given the average spacecraft distance of 1.46×10^6 km
480 and the NIMS pixel field of view of $500 \mu\text{rad} \times 500 \mu\text{rad}$. This resolution – comparable to
481 that acquired from Earth with 0.25-arcsec seeing near jovian opposition – allows a
482 detailed study of Jupiter's spatial and vertical structure.

483

484 To determine the cloudtop altitude, we utilize the well-established radiative transfer
485 algorithms for inhomogeneous atmospheres used previously in preliminary analyses of
486 the Great Red Spot (Baines et al., 1996; Irwin et al., 1999) and, more recently, of other
487 jovian features (Baines et al., 2013). For each point in the GRS mosaic, the cloudtop
488 altitude is derived from a combined analysis of the apparent albedo I/F observed at
489 three wavelengths: (1) the pseudo-continuum wavelength at 1.89 μm , and (2) strong
490 gas absorptions by methane and hydrogen at 1.76 and 2.12 μm , respectively. In this
491 model, the cloud opacity is assumed to be distributed uniformly with pressure (i.e.,
492 unity for the ratio of particle scale height to that of the atmospheric gas), the cloud
493 bottom is assumed to be the NH_3 condensation level at 0.7 bar, and the double Henyey-
494 Greenstein phase function of Tomasko et al. (1978) is assumed for the particles. Below
495 the GRS, underneath an aerosol-free layer extending downward from the 0.7-bar cloud
496 bottom, an optically thick ($\tau_c \gg 1$) lower cloud is assumed placed deep in the
497 atmosphere. Its pressure is found to be nominally near 2.8 bar as determined from 1.6-
498 μm pseudo-continuum observations assuming the single-scattering albedo found at
499 1.89- μm , detailed below. We note that, given that our cloudtop-determining
500 wavelengths are strongly gas-absorbing, the characteristics of the atmosphere below
501 the upper cloud have a only minor effect on the determination of the cloudtop pressure.
502 The zero-altitude pressure value in Fig. 1 is 1 bar and the top of the altitude scale
503 corresponds to about 170 mbar.

504

505 In our analysis, we first determine the single-scattering albedo (ω) at 1.89 μm for a large
506 range of cloud opacities (τ_{Cl}) and cloudtop altitudes (P_{Ct}). We then use these 1.89- μm ω
507 solutions to model 1.76- and 2.12- μm I/Fs over the same range of (τ_{Cl} , P_{Ct}). For H_2 , we
508 use the H_2 pressure-induced absorption formalisms of Borysow (1992) and Birnbaum et
509 al. (1996) for an assumed equilibrium ortho-para H_2 distribution, and the
510 temperature/pressure structure of Lindal et al. (1981). To calculate the methane gas
511 absorption, we use the exponential-sum/correlated-k (Goody et al., 1989; Lacis and
512 Oinas, 1991) with the relevant low-temperature near-IR methane absorption
513 coefficients of Irwin et al. (1996), and assume a methane mixing ratio of 0.0018 as
514 determined by the Galileo Probe Mass Spectrometer experiment (Niemann et al., 1998).
515 The adopted helium abundance is 13.6% (Niemann et al., 1998; von Zahn et al., 1998).
516 Due to the different behavior in absorption as a function of pressure between the 2.12-
517 μm H_2 absorption and the 1.76- μm CH_4 absorption – the former, being a pressure-
518 induced absorption, varies its strength as the square of the pressure while the latter
519 varies its strength linearly – we find tight solutions (uncertainties less than ≈ 10 mbar)
520 for the cloudtop pressures that fit the I/F's at 1.76 and 2.12 μm , including their I/F
521 uncertainties.

522

523 References

524

- 525 Achterberg, R. K., Conrath, B. J., Gierasch, P. J., 2006. Cassini CIRS retrievals of
526 ammonia in Jupiter's upper troposphere. *Icarus*. 182, 169-180.
- 527 Baines, K. H., Carlson, R. W., Kamp, L. W., 2002. Fresh ammonia ice clouds in Jupiter -
528 I. Spectroscopic identification, spatial distribution, and dynamical implications.
529 *Icarus*. 159, 74-94.
- 530 Baines, K. H., Carlson, R. W., Orton, G. S., 1996. The vertical and dynamical structure of
531 the Great Red Spot as determined by Galileo/NIMS. *Bull. Amer.Astron.Soc.*, Vol.
532 28, pp. 1136.
- 533 Baines, K. H., et al., 2013. The temporal evolution of the July 2009 Jupiter impact cloud.
534 *Planetary and Space Science*. 77, 25-39.
- 535 Birnbaum, G., Borysow, A., Orton, G. S., 1996. Collision-induced absorption of H_2 - H_2
536 and H_2 -He in the rotational and fundamental bands for planetary applications.
537 *Icarus*. 123, 4-22.
- 538 Borysow, A., 1992. New model of collision-induced infrared absorption spectra of H_2 -He
539 pairs in the 2-2.5 micron range at temperatures from 20 to 300 K - an update.
540 *Icarus*. 96, 169-175.
- 541 Brown, R. H., et al., 2004. The Cassini visual and infrared mapping spectrometer (VIMS)
542 investigation. *Space Science Reviews*. 115, 111-168.
- 543 Capaccioni, F., Coradini, A., Cerroni, P., Amici, S., 1998. Imaging spectroscopy of
544 Saturn and its satellites : vims-v onboard Cassini. *Planet. Space Sci*. 46, 1263-
545 1276.

546 Chadra, M. S., Flores, J. J., Lawless, J. G., Ponnampereuma, C., 1971. Organic synthesis
547 in a simulated jovian atmosphere - II. *Icarus*. 15, 39-44.

548 Chen, F. Z., Judge, D. L., Wu, C. Y. R., Caldwell, J., 1999. Low and room temperature
549 photoabsorption cross sections of NH₃ in the UV region. *Planet. Space Sci.* 47,
550 261-266.

551 Cheng, B.-M., et al., 2006. Absorption cross sections of NH₃, NH₂D, NHD₂, and ND₃ in
552 the spectral range 140-220 nm and implications for planetary isotopic
553 fractionation. *Astrophys. J.* 647, 1535-1542.

554 Cody, R. B., Laramée, J. A., Durst, H. H., 2005. Versatile new ion source for the analysis
555 of materials in open air under ambient conditions. *Anal. Chem.* 77, 2297-2302.

556 Coradini, A., et al., 2004 CASSINI/VIMS-V at Jupiter: Radiometric calibration test and
557 data results. *Planet. Space Sci.* 52, 661-670.

558 Edgington, S. G., et al., 1999. Ammonia and eddy mixing variations in the upper
559 troposphere of Jupiter from HST Faint Object Spectrograph observations. *Icarus*.
560 142, 342-356.

561 Ferris, J. P., Benson, R., 1981. An investigation of the mechanism of phosphine
562 photolysis. *J. Am. Chem. Soc.* 103, 1922-1927.

563 Ferris, J. P., Bossard, A., Khwaja, H., 1984. Mechanism of phosphine photolysis.
564 Application to jovian photochemistry. *J. Am. Chem. Soc.* 106, 318-324.

565 Ferris, J. P., Chen, C. T., 1975. Photosynthesis of organic compounds in the atmosphere
566 of Jupiter. *Nature*. 258, 587-588.

567 Ferris, J. P., Ishikawa, Y., 1987. HCN and chromophore formation on Jupiter. *Nature*.
568 326, 777.

569 Ferris, J. P., Ishikawa, Y., 1988. Formation of HCN and acetylene oligomers by
570 photolysis of ammonia in the presence of acetylene - Applications to the
571 atmospheric chemistry of Jupiter. *J. Amer. Chem. Soc.* 110, 4306-4312.

572 Ferris, J. P., Khwaja, H., 1985. Laboratory simulations of PH₃ photolysis in the
573 atmospheres of Jupiter and Saturn. *Icarus*. 62, 415-424.

574 Ferris, J. P., Morimoto, J. Y., 1981. Irradiation of NH₃-CH₄ mixtures as a model of
575 photochemical processes in the Jovian planets and Titan. *Icarus*. 48, 118-126.

576 Ferris, J. P., Morimoto, J. Y., Benson, R., Bossard, A., 1982. Photochemistry of NH₃,
577 CH₄, and PH₃. Possible applications to the jovian planets. *Origins of Life*. 12,
578 261-265.

579 Filacchione, G., 2006. Calibrazioni a terra e prestazioni in volo di spettrometri ad
580 immagine nel visibile e nel vicino infrarosso per l'esplorazione planetaria. Vol.
581 PhD. Università Federico II, Napoli, Italy.

582 Fletcher, L. N., et al., 2010. Thermal structure and composition of Jupiter's Great Red
583 Spot from high-resolution thermal imaging. *Icarus*. 208, 306-328.

584 Goody, R., West, R. A., Chen, L., Crisp, D., 1989. The correlated-k method for radiation
585 calculations in nonhomogeneous atmospheres. *J. Quant. Spect. Radiative Trans.*
586 42, 539-550.

587 Griffith, C. A., Bezaud, B., Owen, T., Gautier, D., 1992. The tropospheric abundances of
588 NH₃ and PH₃ in Jupiter's Great Red Spot, from *Voyager IRIS* observations. *Icarus*.
589 98, 82-93.

590 Guillemin, J. C., El Chaouch, S., Bouayad, A., Janati, T., 2001 Partial pressures and
591 nature of products. Application to the photolysis of PH₃ and NH₃ in the

592 atmosphere of Jupiter and Saturn. *Space Life Sciences: Life in the Solar System:*
 593 *Prebiotic Chemistry, Chirality and Space Biology*, pp. 245-253.
 594 Guillemin, J. C., Janati, T., Lassalle, L., 1995. Photolysis of phosphine in the presence of
 595 acetylene and propyne, Gas-mixtures of planetary interest. *Adv. Space Res.* 16,
 596 85-92.
 597 Guillemin, J. C., LeSerre, S., Lassalle, L., 1997 Regioselectivity of the photochemical
 598 addition of phosphine to unsaturated hydrocarbons in the atmospheres of Jupiter
 599 and Saturn. *Life Sciences: Complex Organics in Space*, pp. 1093-1102.
 600 Hapke, B., 1993. *Theory of reflectance and emittance spectroscopy*. Cambridge
 601 University Press, Cambridge.
 602 Irwin, P. G. J., Calcutt, S. B., Taylor, F. W., Weir, A. L., 1996. Calculated k distribution
 603 coefficients for hydrogen- and self-broadened methane in the range 2000-9500
 604 cm⁻¹ from exponential sum fitting to band-modelled spectra. *Journal of*
 605 *Geophysical Research.* 101, 26137-26154.
 606 Irwin, P. G. J., et al., 2004. Retrievals of jovian tropospheric phosphine from
 607 Cassini/CIRS. *Icarus.* 172, 37-49.
 608 Irwin, P. G. J., et al., 1999. Jovian atmospheric studies with the Galileo near infrared
 609 mapping spectrometer: An update. *Adv. Space Res.* 23, 1623-1632.
 610 Kaye, J. A., Strobel, D. F., 1983. HCN formation on Jupiter - The coupled
 611 photochemistry of ammonia and acetylene. *Icarus.* 54, 417-433.
 612 Keane, T. C., 1995. *The Coupled Photochemistry of Ammonia and Acetylene:*
 613 *Applications to the Atmospheric Chemistry on Jupiter*. Ph.D.Thesis. Rensselaer
 614 Polytechnic Institute, Troy, New York.
 615 Keane, T. C., Yuan, F., Ferris, J. P., 1996. Potential Jupiter atmospheric constituents:
 616 Candidates for the mass spectrometer in the Galileo Entry Probe. *Icarus.* 122,
 617 205-207.
 618 Khare, B. N., Sagan, C., 1973. Red clouds in reducing atmospheres. *Icarus.* 20, 311-321.
 619 Lacleis, A. A., Oinas, V., 1991. A description of the correlated-k distribution method for
 620 modelling nongray gaseous absorption, thermal emission, and multiple scattering
 621 in vertically inhomogeneous atmospheres. *Journal of Geophysical Research.* 96,
 622 9027-9064.
 623 Lara, L.-M., Bézard, B., Griffith, C. A., Lacy, J. H., Owen, T., 1998. High-resolution 10-
 624 micronmeter spectroscopy of ammonia and phosphine lines on Jupiter. *Icarus.*
 625 131, 317-333.
 626 Lewis, J. S., Prinn, R. G., 1970. Jupiter's clouds: Structure and composition. *Science.*
 627 169, 472-473.
 628 Lindal, G. F., et al., 1981. The atmosphere of Jupiter - an analysis of the Voyager radio
 629 occultation measurements. *Journal of Geophysical Research.* 86, 8721-8727.
 630 Martonchik, J. V., Orton, G. S., Appleby, J. F., 1984. Optical properties of NH₃ ice from
 631 the far infrared to the near ultraviolet. *Appl. Optics.* 23, 541-547.
 632 Miller, E. A., et al., 1996. The visual and infrared mapping spectrometer for Cassini.
 633 *Proc. SPIE.* 2803, 206-220.
 634 Molton, P. M., Ponnampuruma, C., 1974. Organic synthesis in a simulated jovian
 635 atmosphere. III. Synthesis of aminonitriles. *Icarus.* 21, 166-174.

636 Mordaunt, D. H., Ashfold, M. N. R., Dixon, R. N., Loffler, P., Schneider, L., Welge, K.
637 H., 1998. Near threshold photodissociation of acetylene. *J. Chem. Phys.* 108, 519-
638 526.

639 Moses, J. I., Visscher, C., Keane, T. C., Sperier, A., 2010. On the abundance of non-
640 cometary HCN on Jupiter. *Faraday Disc.* 147, 103-136.

641 Nakayama, T., Watanabe, T., 1964. Absorption and photoionization coefficients of
642 acetylene, propyne, and 1-butene. *J. Chem. Phys.* 40, 558-561.

643 Niemann, H. B., et al., 1998. The composition of the Jovian atmosphere as determined by
644 the Galileo probe mass spectrometer. *Journal of Geophysical Research.* 103,
645 22831-22846.

646 Orton, G. S., 1975. Spatially resolved absolute spectral reflectivity of Jupiter: 3390-8400
647 A. *Icarus.* 26, 159-174.

648 Owen, T., Mason, H. P., 1969. New studies of Jupiter's atmosphere. *J. Atmos. Sci.* 26,
649 870-873.

650 Peek, B. M., 1958. *The Planet Jupiter.* Faber & Faber, London.

651 Pérez-Hoyos, S., Sánchez-Lavega, A., Hueso, R., García-Melendo, E., Legrarreta, J.,
652 2009. The jovian anticyclone BA III. Aerosol properties and color change. *Icarus.*
653 203, 516-530.

654 Ponnampertuma, C., 1976. The organic chemistry and biology of the atmosphere of the
655 planet Jupiter. *Icarus.* 29, 321-328.

656 Prinn, R. G., 1970. UV radiative transfer and photolysis in Jupiter's atmosphere. *Icarus.*
657 13, 424-436.

658 Prinn, R. G., Lewis, J. S., 1975. Phosphine on Jupiter and implications for the Great Red
659 Spot. *Science.* 190, 274-276.

660 Sada, P. V., Beebe, R. F., Conrath, B. J., 1996. Comparison of the structure and dynamics
661 of Jupiter's Great Red Spot between the Voyager 1 and 2 encounters. *Icarus.* 119,
662 311-335.

663 Sagan, C., Khare, B. N., 1971. Experimental jovian photochemistry: Initial results.
664 *Astrophys. J.* 168, 563-569.

665 Sagan, C., Lippincott, E. R., Dayhoff, M. O., Eck, R. V., 1967. Organic molecules and
666 the coloration of Jupiter. *Nature.* 213, 273-274.

667 Sagan, C., Miller, S. L., 1960. Molecular synthesis in simulated reducing planetary
668 atmospheres (abstract). *Astron. J.* 65, 499.

669 Sill, G. T., 1975 The chemistry of the jovian cloud colors. In: T. Gehrels, (Ed.), *Jupiter.*
670 Univ. Arizona Press, Tucson, pp. 372-383.

671 Simon-Miller, A. A., Banfield, D., Gierasch, P. J., 2001a. Color and the vertical structure
672 in Jupiter's belts, zones, and weather systems. *Icarus.* 154, 459-474.

673 Simon-Miller, A. A., Banfield, D., Gierasch, P. J., 2001b. An HST study of jovian
674 chromophores. *Icarus.* 149, 94-106.

675 Simon-Miller, A. A., Carlson, R. W., Sanchez-Lavega, A., 2013. An intense red jovian
676 cyclone: Another key fo finding the chromophores. *Icarus.* Submitted.

677 Simon, A. A., Wong, M. H., Orton, G. S., 2015. First results from the Hubble OPAL
678 program: Jupiter in 2015. *Astrophys. J.* 812:55.

679 Socrates, G., 2001. *Infrared and Raman Characteristic Group Frequencies.* Wiley,
680 Chichester.

681 Strycker, P. D., Chanover, N. J., Simon-Miller, A. A., Banfield, D., Gierasch, P. J., 2011.
682 Jovian chromophore characteristics from multispectral HST images. *Icarus*. 215,
683 552-583.

684 Taylor, F. W., Atreya, S., Encrenaz, T., Hunten, D. M., Irwin, P. G. J., Owen, T. C., 2004
685 The composition of the atmosphere of Jupiter. In: F. Bagenal, T. E. Dowling, W.
686 B. McKinnon, (Eds.), *Jupiter*. Cambridge University Press, Cambridge, pp. 59-78.

687 Tokunaga, A. T., Ridgway, S. T., Knacke, R. F., 1980. High spatial and spectral
688 resolution 10-micron observations of Jupiter. *Icarus*. 44, 93-101.

689 Tomasko, M. G., West, R. A., Castillo, N. D., 1978. Photometry and polarimetry of
690 Jupiter at large phase angles. I - Analysis of imaging data of a prominent belt and
691 a zone from Pioneer 10. *Icarus*. 33, 558-592.

692 Toon, O. B., Ackerman, T. P., 1981. Algorithms for the calculation of scattering by
693 stratified spheres. *Appl. Optics*. 20, 3657-3660.

694 Tsukada, M., Oka, T., Shida, S., 1972. Photochemical and radiation-induced reactions of
695 acetylene and hydrogen sulfide mixture. Synthesis of thiophene. *Chemistry Lett*.
696 1972, 437-440.

697 Van De Hulst, H. C., 1980. *Multiple Light Scattering and Radiative Transfer*, Vol. 2.
698 Academic Press, New York.

699 Visconti, G., 1981. Penetration of solar UV radiation and photodissociation in the Jovian
700 atmosphere. *Icarus*. 45, 638-652.

701 von Zahn, U., Hunten, D. M., Lehmacher, G., 1998. Helium in Jupiter's atmosphere:
702 Results from the Galileo probe helium interferometer experiment. *Journal of*
703 *Geophysical Research*. 103, 22815-22830.

704 West, R. A., Strobel, D. F., Tomasko, M. G., 1986. Clouds, aerosols, and photochemistry
705 in the Jovian atmosphere. *Icarus*. 65, 161-217.

706 Woeller, F., Ponnampertuma, C., 1969. Organic synthesis in a simulated jovian
707 atmosphere. *Icarus*. 10, 386-392.

708

709

710
711
712
713
714
715
716
717
718
719
720
721
722
723
724
725
726
727
728
729
730
731
732
733
734
735
736
737
738
739
740

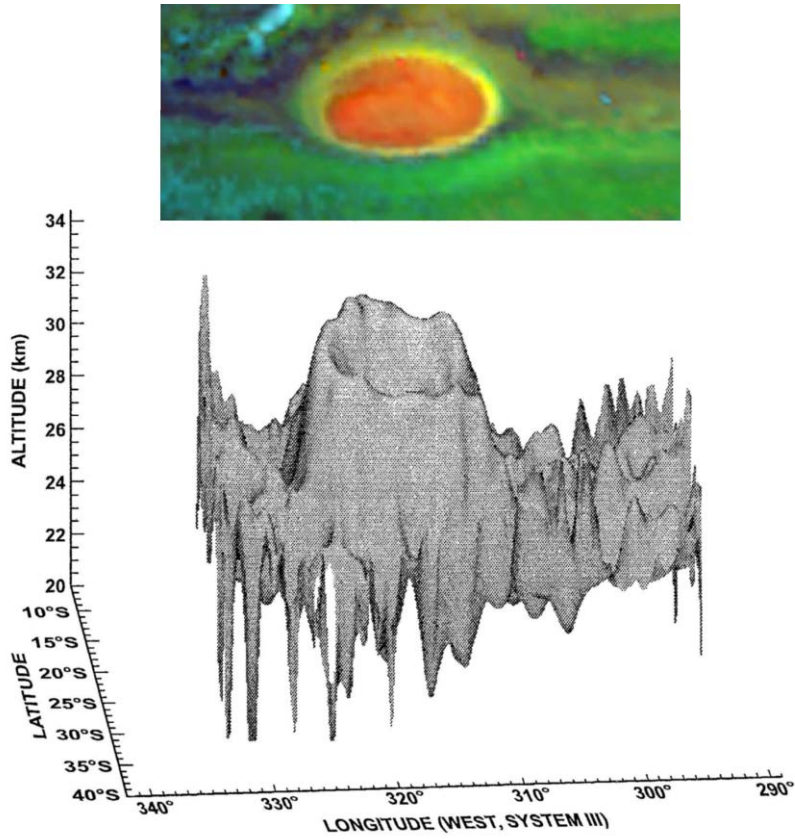
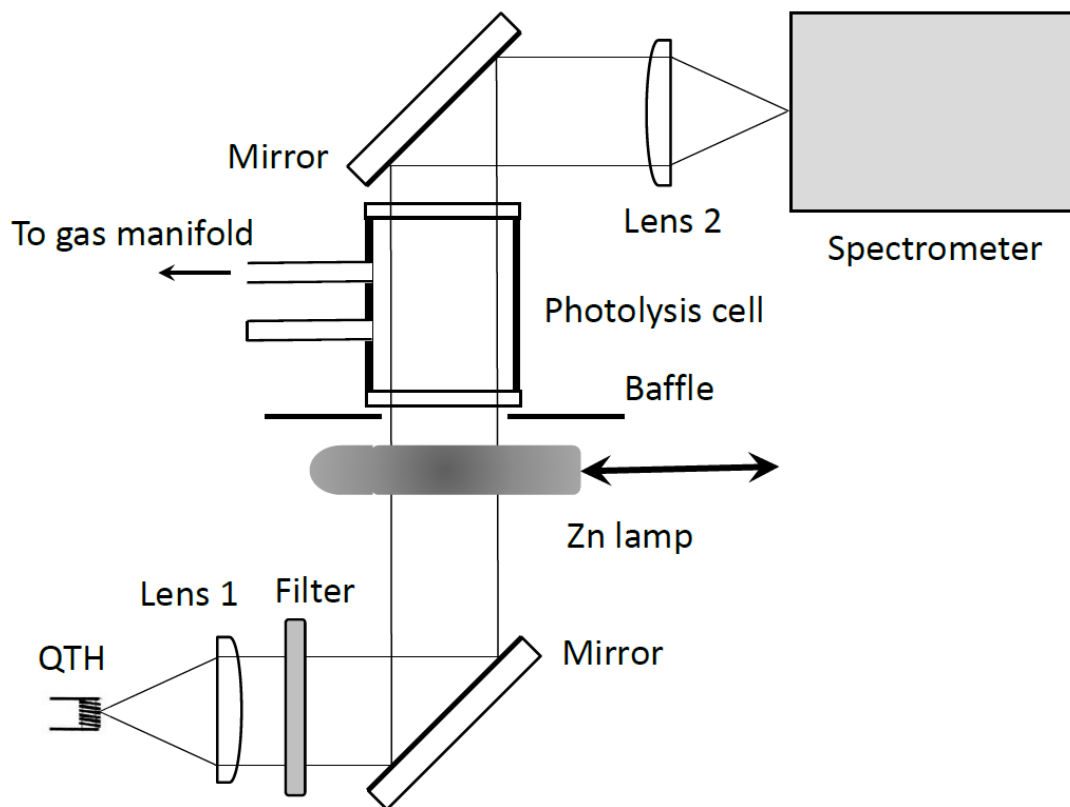


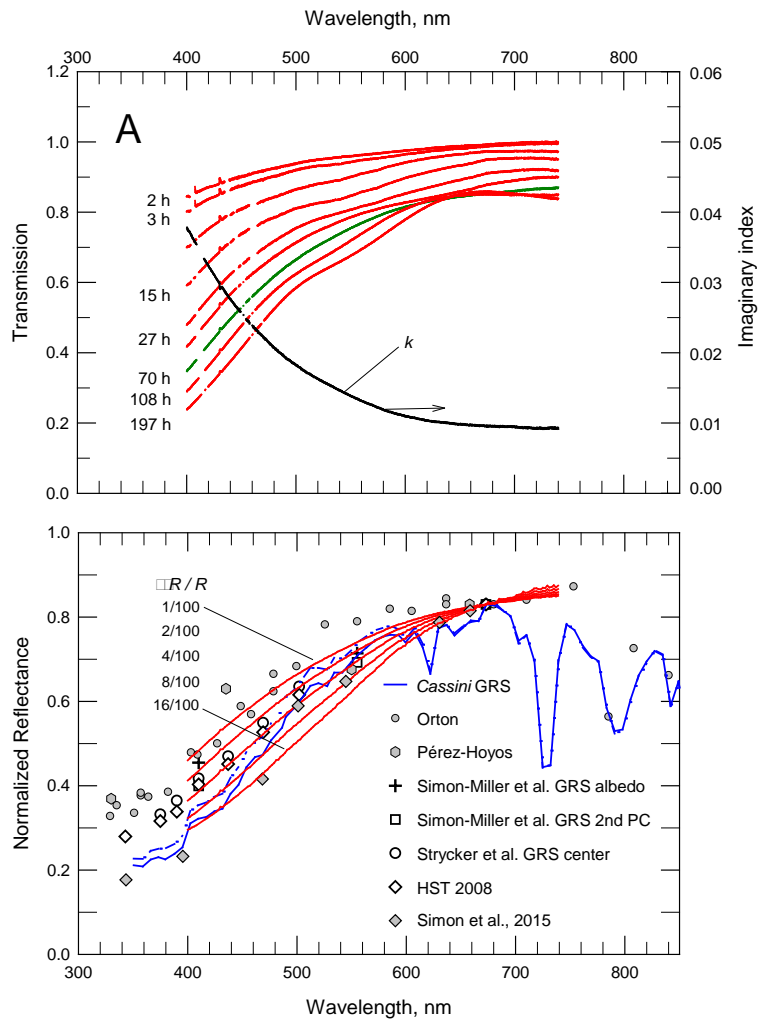
Fig. 1. *Galileo* NIMS false color image of the GRS and corresponding altimetry map. The analysis method to obtain these results is described in the Appendix. In the image, red corresponds to the radiance at 2.06 μm and is in indicator of altitude. Altitudes are relative to the 1-bar level.

741
742
743
744



745
746
747
748
749
750
751
752
753
754
755
756
757
758
759
760
761
762
763
764

Fig. 2. Experimental arrangement used in the photolysis measurements. The zinc lamp photolyzes NH_3 in the gas cell that also contains C_2H_2 . A resulting yellow-orange film is deposited on the inner surface closest to the lamp. The transmission of the film is measured by removing the Zn lamp and using collimated visible light from a quartz-tungsten-halogen lamp (QTH). The light passing through an order sorting filter, a baffle, the photolysis cell, and then is focused on the entrance slit of a grating spectrometer. The photolysis cell and gas manifold form a closed system but occasionally small samples of gas are withdrawn for analysis.



765
766
767
768
769
770
771
772
773
774
775
776
777
778
779
780
781

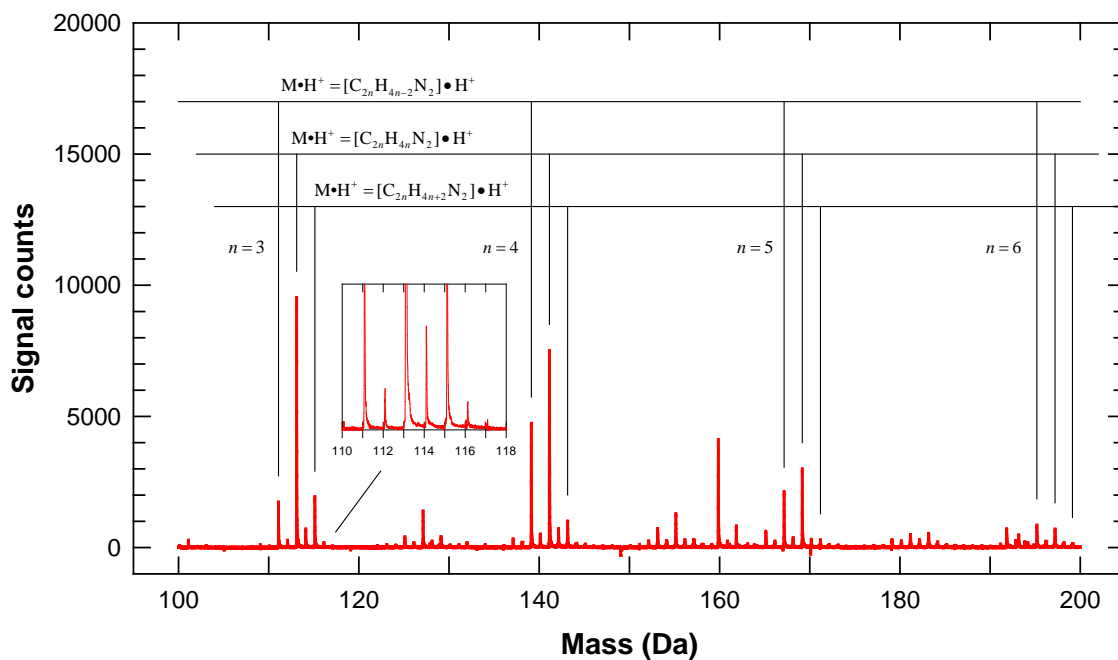
Fig. 3. Laboratory spectra of the photolysis products (upper panel A). Transmission spectra are shown for different average exposure times for Experiment No. 3 (Table 1). The data outages and small glitches correspond to gain-state changes. The 70-hour curve, shown in green, shows minimal effect from channel fringes and was used to derive the chromophore's imaginary index of refraction, shown as the black curve. Panel B shows model calculations (in red) of the GRS reflectivity using the derived index, Mie scattering calculations for spheres with various thicknesses of chromophore coating, and radiative transfer approximations. The calculated reflectivities are consistent with ground-based data obtained by Orton (1975), HST measurements (Simon-Miller et al., 2001b; Pérez-Hoyos et al., 2009; Strycker et al., 2011; Simon et al., 2015) and *Cassini* VIMS spectra. The central pixel of the VIMS observation is shown as the solid blue line; The dashed blue line is the average of central and adjoining eastern and western pixels. The *Cassini* and HST 2008 data are discussed in the text and the HST 2008 image is shown in Fig. 4B.



782
783
784
785
786
787
788
789

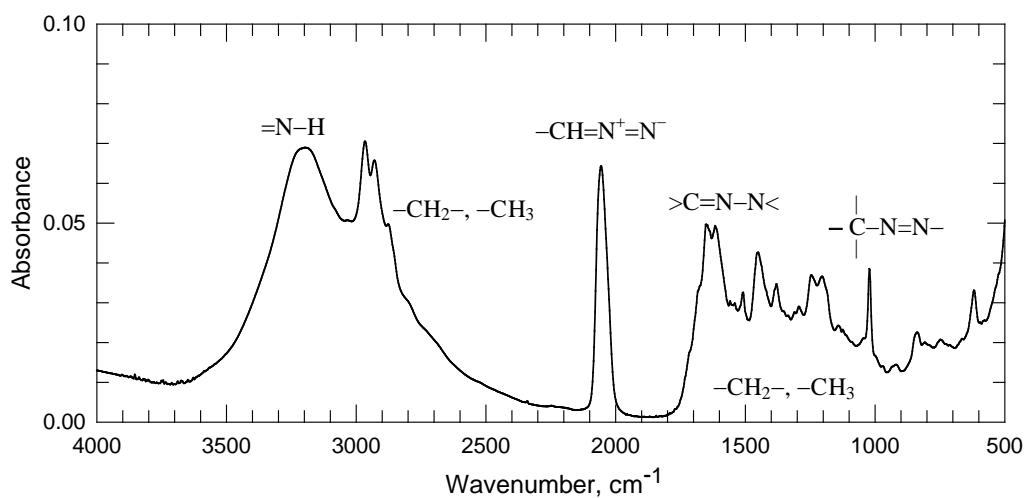
Fig. 4. Color comparison of the laboratory-produced chromophore on SiO_2 microspheres in transmission (A. at left) with a *Hubble* image (B, at right) using red, green, and blue spectral reflectivities (I/F) images to generate true colors. Note the GRS's dark center and surrounding annulus. The non-uniformity in the laboratory image in A is due to clumping of the SiO_2 powder.

790



791
792
793
794
795
796
797
798
799

Fig. 5 DART high-resolution mass spectrum of the chromophore-containing deposit produced in Experiment No. 1. Four groups of 3 main members, each containing two N atoms, are shown and are interpreted as combinations of aliphatic azine, azo, and diazo hydrocarbons. The inset shows details of the mass peak profiles and presence of heavier C- and N-isotopes.



800
 801 Fig. 6. Infrared spectrum of the experimental chromophore-bearing residue, showing
 802 features attributed to the functional groups imine ($=N-H$), methyl ($-CH_3$), and
 803 methylene ($-CH_2-$). The di-nitrogen functional groups are suggested as diazo
 804 compounds ($RR'C=N^+=N^-$) from the band at 2056 cm^{-1} , azines and hydrazones
 805 ($>C=N-N<$) from the $C=N$ stretch transition near 1650 cm^{-1} , and azo groups ($R-N=N-R'$)
 806 from the $C-N$ stretch band at about 1020 cm^{-1} . R represents hydrocarbon radicals.